Edith Cowan University

Research Online

8-15-2023

Hydrogen, carbon dioxide, and methane adsorption potential on Jordanian organic-rich source rocks: Implications for underground H2 storage and retrieval

Amer Alanazi

Hussein Rasool Abid
Edith Cowan University

Muhammad Usman

Muhammad Ali
Edith Cowan University

Alireza Keshavarz
Edith Cowan University

See next page for additional authors

Alanazi, A., Abid, H. R., Usman, M., Ali, M., Keshavarz, A., Vahrenkamp, V., ... & Hoteit, H. (2023). Hydrogen, carbon dioxide, and methane adsorption potential on Jordanian organic-rich source rocks: Implications for underground H2 storage and retrieval. *Fuel*, 346, Article 128362. https://doi.org/10.1016/j.fuel.2023.128362
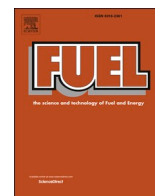
Authors

Amer Alanazi, Hussein Rasool Abid, Muhammad Usman, Muhammad Ali, Alireza Keshavarz, Volker Vahrenkamp, Stefan Iglauer, and Hussein Hoteit

Full Length Article

Hydrogen, carbon dioxide, and methane adsorption potential on Jordanian organic-rich source rocks: Implications for underground H$_2$ storage and retrieval

Amer Alanazi [a],[*], Hussein Rasool Abid [b],[c], Muhammad Usman [a], Muhammad Ali [a],[b], Alireza Keshavarz [b], Volker Vahrenkamp [a], Stefan Iglauer [b], Hussein Hoteit [a]

[a] *Physical Science and Engineering Division, King Abdullah University of Science and Technology (KAUST), Thuwal 23955, Saudi Arabia*
[b] *Petroleum Engineering Discipline, School of Engineering, Edith Cowan University, 270 Joondalup Dr, Joondalup 6027, WA, Australia*
[c] *Environmental Department, Applied Medical Science, University of Karbala, Karbala, Iraq*

ARTICLE INFO

ABSTRACT

Hydrogen (H$_2$) storage in geological formations offers a potential large-scale solution suitable for an industrial-scale hydrogen economy. However, the presence of organic residuals can significantly influence the H$_2$ storage efficiency, as well as cushion gas performance, such as CO$_2$ and CH$_4$, injected to maintain healthy reservoir pressure. Thus, the H$_2$ storage efficiency and cushion gas selectivity were thoroughly investigated in this work based on H$_2$, CO$_2$, and CH$_4$ adsorption measurements using, for the first time, actual organic-rich carbonate-rich Jordanian source rock samples (TOC = 13 % to 18 %), measured at 60 °C temperature and a wide range of pressure (0.1 – 10.0 MPa). Initially, the samples were characterized using various analytical methods. Results demonstrated that H$_2$ adsorption capacities reached up to 0.47 mol/kg at 9.0 MPa. The measured adsorption of CO$_2$ was four times higher than H$_2$. An increase in TOC significantly decreased H$_2$ adsorption compared to CO$_2$ and CH$_4$. Additionally, CO$_2$ demonstrated preferential behavior as a cushion gas compared to CH$_4$, attributed mainly to the calcite content and presence of carboxyl and sulfonyl groups. This study provides fundamental data for understanding H$_2$ potential storage issues in an organic-rich rock formation and thus aids in the industrial implementation of an H$_2$ supply chain.

1. Introduction

Hydrogen is a clean fuel recognized as a promising alternative to fossil fuels in support of the global decarbonization plans to effectively reduce the negative impact of carbon emissions on the climate [1–4]. Hydrogen supports alternative sources of clean energy production, such as wind turbines and solar systems, while helping to overcome their intermittency problem and the off-seasonal supply nature [5,6]. However, an industrial-scale expansion of a hydrogen-based economy requires the existence of a vast storage medium, which is still the foremost hurdle to achieve [2,7–13]. Therefore, several solutions for hydrogen storage have been proposed, including underground hydrogen storage (UHS) in geological formations, such as salt caverns, saline aquifers, and depleted oil and gas reservoirs [3,9–12,14–21].

Geological formations represent natural structures that can provide vast storage capacities for future strategic energy demands [9,22,23].

Among them are those depleted hydrocarbon-prone conventional and unconventional reservoirs structurally deeper than the other salt caverns and saline aquifers and characterized by formations with tight pore networks (i.e., nano to mesopore) [24]. These reservoirs are potentially regarded as a suitable option since they represent pressurized natural containers for gas storage and can adsorb large amounts of hydrogen (H$_2$), carbon dioxide (CO$_2$), and methane (CH$_4$), with a low risk of leakage [25–27]. Higher reservoir pressure implies that the gas can be readily withdrawn [28]. Typically, underground H$_2$ storage requires a volume of a secondary gas to be maintained in the reservoir before the injection of H$_2$ for storage, which is referred to as "cushion gas" [29]. Notably, the cushion gas manages the reservoir pressure and provides the required energy for the H$_2$ extraction. The cushion gas can be either the same gas or preferably a denser gas than H$_2$, such as CO$_2$ and CH$_4$ [17,30–36]. The maximum extracted gas volume from a reservoir represents the storage capacity, also known as the "working gas" [19,37].

---

* Corresponding author.
 E-mail address: Amer.alanazi@kaust.edu.sa (A. Alanazi).

The main trapping mechanisms that govern the immobilization of the buoyant H_2 during UHS are the residual capillary trapping within a reservoir rock and structural trapping caused by an impermeable sealing caprock [38–41]. These trapping mechanisms are highly influenced by the H_2 adsorption capacity inside a rock pore structure. Recent studies have depicted the significant role of H_2 adsorption on the surface of coal seam and clay-rich rock samples[26,42–46]. The concept of adsorption trapping is to store H_2, which is adsorbed on the rock surface during the storage process and extracted by reducing the pressure during the retrieval process. In standard experimental procedures, the adsorbed gas is also referred to as "absorbed", "sorbed", and "dissolved" gas [47]. Thus, the adsorption isotherms used here denote any state of the gas determined by measuring the gas uptake by a solid, compared to a reference "non-adsorbing" gas (i.e., helium) at different pressure and temperature conditions.

Assessing the amounts of adsorbed gas and adsorption capacity of a rock pore system is challenging and requires a detailed investigation of various controlling parameters [42,48]. The gas adsorption capacity on a rock surface is typically influenced by the operating pressure, temperature, rock elemental and mineral composition, rock pore structure, surface area, and total organic content (TOC) [42,49]. Some publications have linked the decrease in the gas adsorption capacity to the increase in the pore size [50–53]. While, other researchers have reported that gas adsorption–desorption capacities in calcareous and argillaceous shale rocks are mostly influenced by their total organic content (TOC) and thermal maturity [47,49,54–57]. Moreover, H_2 adsorption on synthesized eagle-ford shales saturated with humic acid showed an increased adsorption capacity with pressure [46]. The findings showed that the organic presence can enhance the H_2 geological storage through improving its adsorption on reservoir rock surface, which in turn affects the rock wettability characteristics [58–60].

On the other hand, high organic content is undesirable in caprocks as they negatively affect structural trapping [61]. They can significantly affect the rock wettability in becoming less hydrophilic, which reduces the caprock's ability to prevent H_2 plume migration by reducing capillary entry pressure exerted by the fluids within a caprock against the buoyant H_2 [15,58,62,63]. Thus, it is crucial to study the impact of organics that actually exist in reservoir/cap rocks and evaluate their influence on the rock-wetting characteristics, H_2 trapping mechanisms, sealing efficiency, and storage security in the context of UHS [39,64].

In the literature, the H_2 adsorption behaviour on actual organic-rich rocks has been scarcely reported [49,65,66]. In this work, the different adsorption behaviors of H_2, CO_2, and CH_4 were measured on immature organic-rich carbonate-rich (i.e., calcareous) source rocks from Jordan, known as Jordanian oil shale. The Jordanian oil shale have been typically used to study several maturity characteristics of the source rock and many other geological, economic, geochemical, and environmental aspects [67–74]. However, we used the Jordanian carbonate-rich samples which are naturally rich with organics, to study for the first time the influence of actual organics on H_2 underground storage and cushion gas selectivity between CO_2 and CH_4 demonstrated at moderate pressures and varying TOC. Therefore, this work provides a fundamental concept and technical insight on UHS concerning organic matter to aid a large-scale implementation of a H_2 economy.

2. Jordanian oil shale

The Jordanian source rocks correspond to the Muwaqqar Chalk-Marl (MCM) formation, deposited during the Late Cretaceous to Early Paleocene time [75], as displayed in Fig. 1. During this time, Jordan was located at the southern margin of the NeoTethys Ocean. The global sea-level rise led to the progression of the NeoTethys Ocean over the south and east of the Arabian plate [76]. This progression led to the formation of carbonate platform sequences, including thick limestone, marl, and chalk deposits in the central and southern parts of Jordan [77], Fig. 1b. During the Late Eocene time, the Arabian plate moved northward against the Eurasian plate, resulting in the closure of the NeoTethys ocean and the termination of the shallow marine platform sequence deposition [76].

The MCM formation consists of marl, chalk, and marly to phosphatic
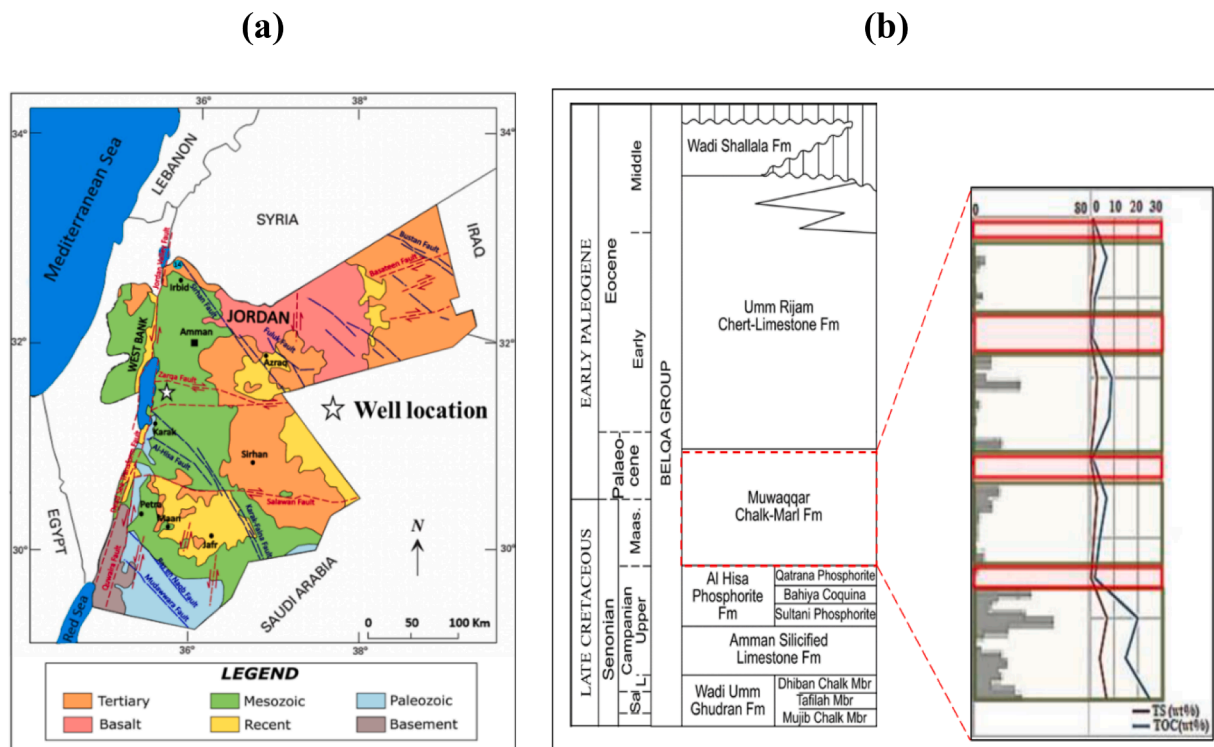

(a) **(b)**

Fig. 1. Information on Jordan source rocks – a) geological map of Jordan showing the drilled well location and b) Generalized stratigraphic column showing significant occurrences from Late Cretaceous to Early Paleogene (modified after Powell and Moh'd, 2011 and Abu-Mahfouz et al., 2019).

limestone and chert beds interbedded with bituminous mudrocks. The organic-rich carbonate mudrock interval was deposited in reducing conditions from the sedimentation of algal organic matter produced in near-surface marine waters [67,77,78].

The Jordanian source rocks, characterized as type II/IIS kerogen, are amongst the richest source rocks globally, with TOC as high as 30 %. However, the Jordanian source rocks generally are thermally immature and have not been reported to produce hydrocarbons on an economic scale. For this study, four samples were selected at different depths from a well drilled in the North-west of Jordan at the location depicted in Fig. 1a.

3. Experimental methods

3.1. Pyrolysis measurements

The four samples were grounded to powders of a particle size between 40 μm and 120 μm. About 50 mg of each sample was analyzed for detailed pyrolysis using RockEval 7S (©Vinci Technologies from Nanterre, France) to measure the organic matter's richness and maturity. The methodological and assessment criteria are already described in [79 and 80]. The obtained parameters from this analysis include S1, S2, S3, T_{max}, and Sulfur content. S1 (mgHC/gRock) signifies the amount of free hydrocarbons present without thermal cracking of the kerogen at about 300 °C. S2 (mgHC/gRock) shows the amount of hydrocarbons released due to thermal cracking from 300 to 600 °C, whereas S3 (mgCO$_2$/gRock) indicates the amount of CO$_2$ released during the programmed pyrolysis. T_{max} (°C) refers to the temperature for the maximum peak of S2 and represents the maturity of the source sample. The sulfur content was measured during pyrolysis and oxidation with temperatures up to 1200 °C. The TOC of the rock was determined by oxidation under air, in a second oven, of the residual organic carbon after pyrolysis. Other valuable parameters were also calculated from the obtained parameters, including the H$_2$ index (HI = S2/TOC), the oxygen index (OI = S3/TOC), the production index (PI = S1/(S1 + S2)) and the hydrocarbon potential (S1 + S2). All the results were checked and calibrated by using an IFP Energies Nouvelles (IFPEN) standards.

3.2. Mineralogy, elemental compositions, and thermal decomposition

The Jordanian source rock samples' elemental composition was characterized via Energy-Dispersive X-ray (EDX) mapping and Scanning Electron Microscopy (SEM) measurements using a Hitachi SU3500 Scanning Electron Microscope. In addition, the corresponding mineralogical compositions were assessed through a RAYONS X-ray powder diffraction (XRD) instrument equipped with a cobalt $K\alpha$ radiation source at 40 kV and 40 mA. The powder diffraction patterns and Rietveld refinement were measured with a Rietveld X-ray diffractometer, whereas the amount of each phase was identified semi-quantitatively with High Score Plus software. A thermo-gravimetric analysis (TGA) was also conducted to measure the decomposition temperature of the analyzed samples using the PerkinElmer-Thermo-gravimetric 4000 Analyzer-TGA system.

3.3. Surface functional groups, specific surface area, and pore size

Fourier-Transformed infrared spectroscopy (FTIR) for the wavenumber range of 650 to 4000 cm^{-1} with a PerkinElmer-Spectrometer 100-FT-IR instrument was conducted to characterize the chemical active functional groups on the rock surface. In addition, the surface zeta potential of the samples was measured using a surface zeta potential analyzer by Malvern instruments. The samples were grounded with a blade grinder (700G high speed chinses electric medicine crusher) and sieved to homogeneous particle sizes between 45 μm and 125 μm. Low-pressure nitrogen (N$_2$, 99.999 vol%) adsorption–desorption isotherm measurements were also carried out at 77 K to measure specific surface

area BET (after Brunauer, Emmett, and Teller), pore volume and average pore size of the samples using a Tristar II (3020) instrument.

3.4. Adsorption measurement

The adsorption profiles of CO$_2$ (purity = 99.99 mol%), CH$_4$ (purity = 99.99 mol%), and H$_2$ (purity = 99.995 mol%) were measured at an elevated temperature value of 60 °C and a wide range of pressures (0.1–10.0 MPa) using a PCTpro-2000 adsorption analyzer (Setaram Instrumentation from Hong Kong). The testing temperature was set to 60 °C to represent the average temperature of oil and gas reservoirs in the region [81,82]. The influence of temperature on gas adsorption potential on a formation rock surface has been previously reported [42]. The higher the temperature, the lower is the gas adsorption due to the increase in the kinetic energy of the gas molecules that will attempt to escape from the adsorbed layer to the gas-free phase [83]. The instrument is fully automated and operates based on Sievert's method for measuring the gas adsorption properties of porous materials [44]. Before the experiment, each sieved and ground sample was heated and dried in the oven at 80 °C for 48 hrs, then heated under vacuum at 60 °C for approximately 12 hrs. Experimentally, the measurements in the instrument rely on the pressure variation, which is composed of two parts. More specifically, the fast pressure variation is due to gas expansion in a more extensive volume reservoir. The slower pressure variation can be ascribed to gas adsorption in a sample. Helium (purity = 99.99 mol%, at 4–5 bar) was also used for calibrating the instrument before the adsorption measurements. Helium is considered an inert gas and can reach all the permeable pores of the sample without being adsorbed [84,85]. A specific mass of dry samples (ranging from 0.5 to 1 g), powdered to a particle size between 40 μm and 120 μm, was poured into the sample cell, and the cell was evacuated for at least two hours at the temperature value of 60 °C. Details of the sample preparation procedure have been provided by a previous study [86]. Several tests were repeated thrice, and the average standard deviation was estimated as ± 3 % based on replicate measurements.

4. Results and discussion

### 4.1. Jordan carbonate source rock properties

The Jordan source rock samples showed varying TOC content ranging from 13 % to 18 %. The obtained parameters from RockEval 7S are presented in Table 1. The samples are numbered descending from the highest TOC (Carbonate-1) to the lowest TOC (Carbonate-4), whereas the Hydrogen Index (HI) shows a slight increase with the decrease in the TOC. A modified Van Krevelen diagram is plotted against HI and Oxygen Index (OI) of the analyzed samples, which suggests a Type II kerogen with high Sulfur content (Fig. 2a). Such kerogen type represents organic matter deposition in marine environments under euxinic conditions. A cross-plot between TOC and hydrocarbon potential yield (S1 + S2) characterized the studied source rocks samples as excellent quality (Fig. 2b) was demonstrated. However, the corresponding T_{max} values for these samples are low (approximately average of 419 °C). The low T_{max} values suggest the studied source rock has not reached the optimum thermal maturity window to generate hydrocarbons and is therefore characterized as an immature source rock interval (Fig. 2c). The complex pyrolysis plots for each sample are displayed in **Figures S1 to S4** in **the supplementary information file**.

4.2. Characterization of organic-rich source rock samples

The analyzed Jordan source rock samples were characterized based on the Dunham classification [87]. The samples showed a fine-grain texture with intra-particle porosities. These samples are poorly sorted, ranging from packstone (Carbonate-1, 2, and 3) to wackestone (Carbonate-4), as depicted in SEM in Fig. 3. The acquired SEM images of the

Table 1
RockEval parameters of the selected samples from Jordan source rock.

Sample Name	S1 (mg/g)	S2 (mg/g)	S3 (mg/g)	Tmax (°C)	HI	OI	PI	TOC (%)	Total Sulfur (%)
Carbonate-1	4.96	147.52	1.35	420	822	8	0.03	17.94	3.68
Carbonate-2	4.17	136.69	1.5	419	847	9	0.03	16.15	2.94
Carbonate-3	4.01	127.78	1.22	420	858	8	0.03	14.89	3.09
Carbonate-4	4.41	111.37	1.14	418	861	9	0.04	12.93	3.06
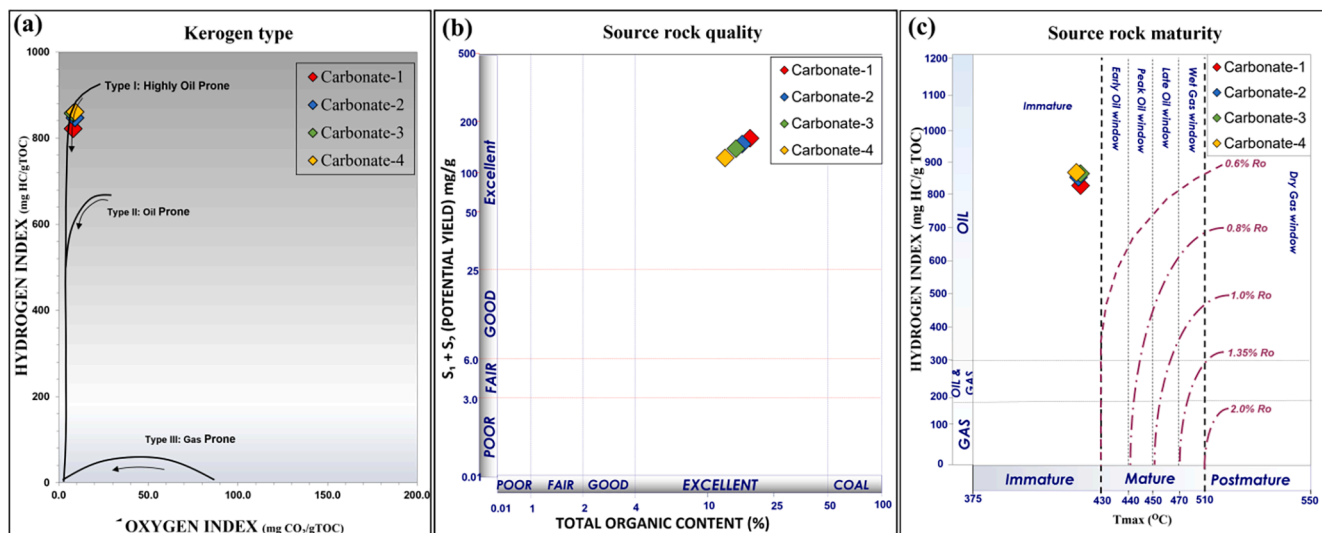
Fig. 2. Analyzed carbonate source rock parameters as derived from RockEval pyrolysis – a) Kerogen type, b) Source rock quality, and c) Source rock maturity.

samples also showed moldic porosities filled with bio-micritized clasts of peloids, plankton foraminifers, bryozoans, and echinoderms which shows the heterogeneity of the packed carbonate source rock.

Additionally, the pore system among all the samples was mainly reduced by syntaxial calcite cement and bio-micrite volume. The packing impact of the different calcified components on the pore system, shown by the SEM images (Fig. 3), is reflected in the pore distribution from the N₂ adsorption/desorption isotherms, as observed in Fig. 4. The average pore size distribution measured from N₂ adsorption–desorption isotherms of all the analyzed samples ranged from 15 to 42 nm (Table 2), indicating a mesoporous system (below 50 nm) with the negligible presence of micropores according to the IUPAC nomenclature [88]. Furthermore, the total volume was measured at relative pressure approaching one, based on the N₂ adsorption–desorption isotherms, as demonstrated in Table 2.

The N₂ adsorption–desorption isotherms indicate the manifestation of Type V isotherm following [89], which can be attributed to the existence of the mesopores with weak interaction of N₂ on the pore surface [90]. The hysteresis in the N₂ desorption isotherms for the four analyzed samples was relatively marginal at lower pressures, as shown in Fig. 5. The hysteresis mainly depends on the mesoporous content and ink-bottle pores so a difference between condensation and evaporation is more likely to happen. More specifically, N₂ molecules were adsorbed on the necks' mesopores' walls. Then, a film of the condensed adsorbed N₂ is made in the mesopores due to the depression impact of the saturated vapor pressure of confined N₂ [89,91]. Among all the analyzed samples, Carbonate-4 showed the most significant hysteresis because of the smaller neck diameter of the mesopores, near the critical diameter N₂ at 77 K (around 4 nm) [26]. Also, TOC content significantly impacted the pore size and pore volume. That is attributed to the fact that the light TOC might work as a template; therefore, porosity was enhanced after evacuating process. Accordingly, the pore volume and pore diameter were significantly increased with increasing the content of TOC while the specific surface area was slightly changed.

### 4.3. Mineralogy, elemental analysis, and surface functional groups

The mineralogy based on XRD analysis revealed that the samples are mainly composed of calcite and quartz with very few traces of phosphate minerals (i.e., berlinite and apatite) (Table 3). Nevertheless, some variations in the mineral abundance between the analyzed samples were detected, as illustrated in **Figure S5** in **the supplementary information** file. The highest calcite abundance was found in the Carbonate-2 sample, with 92 % calcite, and the lowest was found in Carbonate-4, with 44 % calcite. Carbonate-1 and −3 also showed high calcite abundance with 85 % and 73 %, respectively. The XRD also demonstrated a varying amount of quartz in the Jordan source rock samples with Carbonate-1, −2, and −3 possessing a low abundance of quartz (4 to 14 %), whereas Carbonate-4 contains 54 % quartz. The quartz here can be interpreted as biogenic quartz present in the fine matrix of the samples (Fig. 6). The dominant mineralogical composition is calcite except for the Carbonate-4 sample, which has a higher amount of biogenic quartz.

The relative elemental content was observed through EDX mapping of the Jordan source rock samples (Fig. 6). Five points were analyzed for each sample to overcome the heterogeneity of the sample. The acquired results consistently correlate with the XRD results with higher calcium content in the first three carbonate samples, whereas higher silica in the Carbonate-4 sample. The quantitative analysis of the EDX also indicated the carbon (C) concentration following the increase in TOC from RockEval, Fig. 7.

The tested samples were also analyzed with a Thermo-gravimetric analyzer (TGA) to determine their thermal stability and analyze decomposed materials. Four stages with corresponding weight loss (Fig. 8 and **Figures S6 to S9** in **the supplementary information** file) were extracted using a heating rate of 20 °C/min. The first stage is the physical stage, which includes light fraction evaporation from 50 °C to 85 °C. During this stage, the samples lost weight due to releasing moisture content and light-weight hydrocarbons. The second, third, and fourth stages are called the chemical stage, starting beyond 350 °C. This
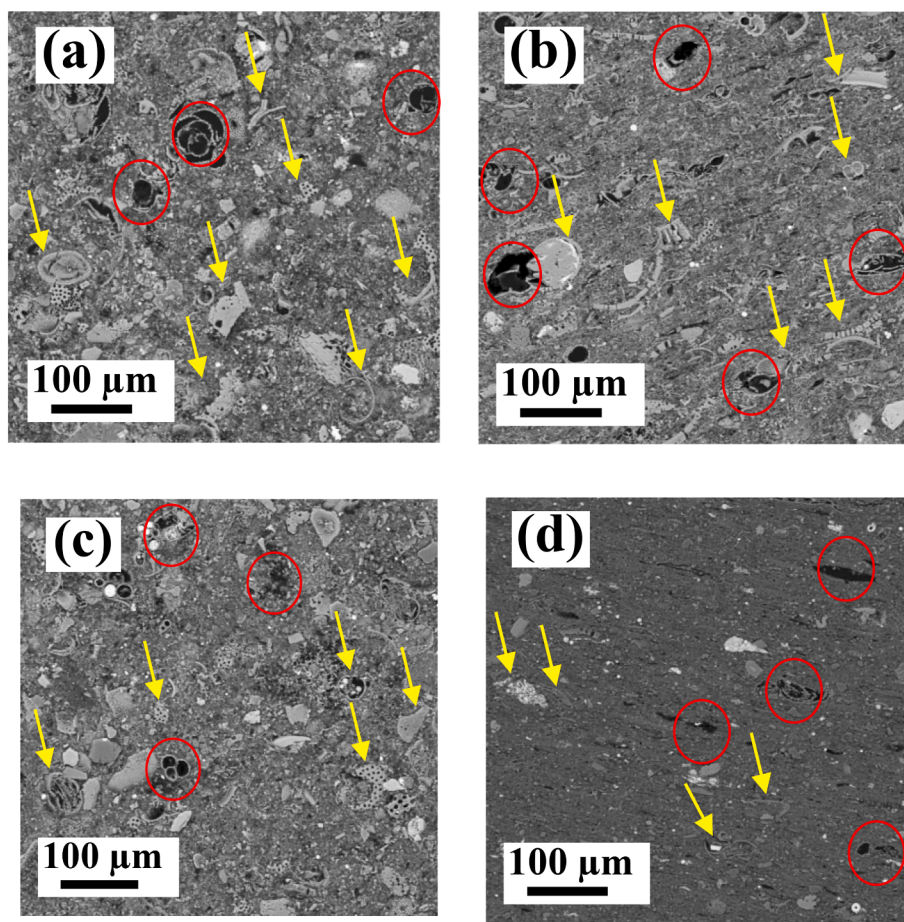
Fig. 3. Scanning Electron Microscopy (SEM) micrographs of the Jordan carbonate mudrock samples – a) Carbonate-1, b) Carbonate-2, c) Carbonate-3, and d) Carbonate-4. Red circles indicate moldic porosity, and the yellow arrows indicate biota. (For interpretation of the references to colour in this figure legend, the reader is referred to the web version of this article.)
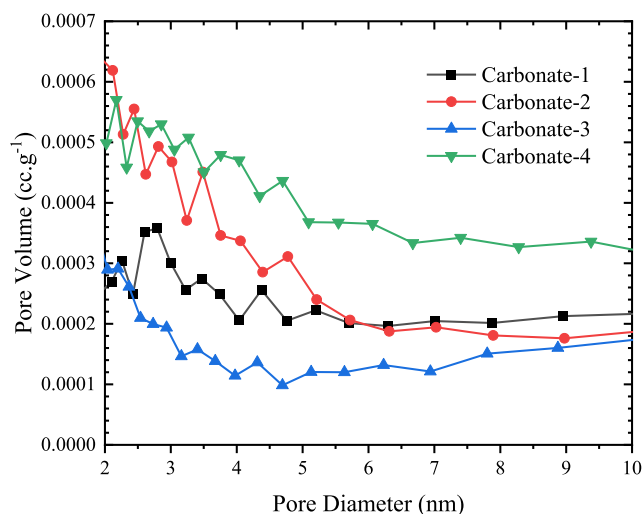
Fig. 4. Pore size distribution of the four analyzed carbonaceous rock samples.

Table 2
Textural properties of the examined samples (Summary of N$_2$ BET).

Sample Name	Carbonate-1	Carbonate-2	Carbonate-3	Carbonate-4
Specific Surface area, m^2/g	3.08	3.68	3.53	3.19
Pore volume, cm^3/g	0.032	0.031	0.024	0.011
Average pore size diameter, nm	41.42	34.60	27.24	14.73
Type of pores (2–50 nm)	Mesopores	Mesopores	Mesopores	Mesopores
Micropores size	None	None	None	None

weight loss is due to the pyrolysis of the remaining kerogen, where the heavy components start cracking and generate gaseous light hydrocarbons. As far as the last stage of weight loss is concerned, it corresponds to the degradation of the carbonates. Considering that the Carbonate-1, −2, and −3 had more calcite content, these samples showed more weight loss than the Carbonate-4 sample, which had relatively lower calcite content.

The FTIR spectra of the carbonate samples are displayed in Fig. 9, which demonstrates a series of peak patterns showing diversified functional groups (refer to Table S1 in the supplementary information file for a detailed description). The spectra primarily characterize band series of the vibrations of calcium carbonate (CO$_3^{-2}$) ions at the band from 690 to 874 cm^{-1} and at the peaks of 2,853 and 2,927 cm^{-1} [92,93]. The highest sharp stretching characteristics of hydrocarbons were demonstrated at 1,420 cm^{-1}, which most likely represents the C—H bonding and refers to the presence of hydrocarbon film on the surface of the rock samples. Additionally, other peaks of CH functional groups might be observed at 2,853 and 2,927 cm^{-1}. There is a broad mountain centered at about 3,622 and 3,699 cm^{-1}, a characteristic of the hydroxyl O—H stretching mode of alcohols. The breadth of this signal stems from the H$_2$ bonding between molecules. Furthermore, bands of free electron
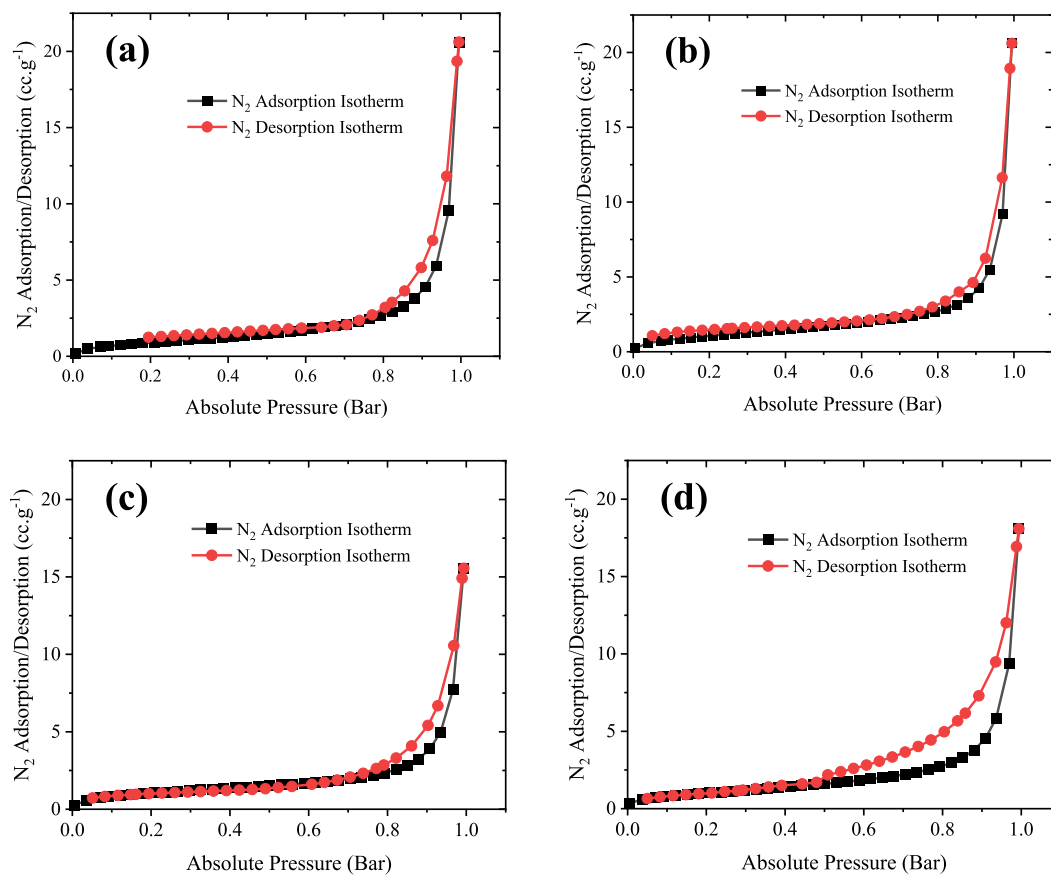
Fig. 5. Nitrogen adsorption–desorption isotherm curves – a) Carbonate-1, b) Carbonate-2, c) Carbonate-3, and d) Carbonate-4.

Table 3

Mineralogy from X-ray powder diffraction (XRD) analysis and TOC from Rock-Eval Pyrolysis for the analyzed samples.

Sample No.	Mineral composition from XRD		
	Mineral phase	Chemical Formula	Abundance %
Carbonate-1	Calcite	$CaCO_3$	85
	Quartz	SiO_2	14
	Berlinite	$Al(PO_4)$	1
Carbonate-2	Calcite	$CaCO_3$	92
	Quartz	SiO_2	4
	Apatite	$Ca_5[PO_4]_3(OH,F,Cl)$	4
Carbonate-3	Calcite	$CaCO_3$	73
	Quartz	SiO_2	14
	Apatite	$Ca_5[PO_4]_3(OH,F,Cl)$	12
	Langite	$Cu_4(SO_4)(OH)_6 \cdot 2H_2O$	1
Carbonate-4	Calcite	$CaCO_3$	44
	Quartz	SiO_2	54
	Apatite	$Ca_5[PO_4]_3(OH,F,Cl)$	1.4
	Berlinite	$Al(PO_4)$	0.5

functional groups were recognized in conjunction with a weak carbonyl peak $C = \ddot{O}$ at 1,798 cm^{-1} and a middle peak of sulfonyl groups $S = \ddot{O}$ at 1,030 cm^{-1}.

The distribution of the peaks varies among the analyzed samples. The carbonate ion (CO_3^{-2}) signals descend from the highest peak in Carbonate-1, followed by Carbonate-2 and 3, to the lowest in Carbonate-4. These results matched the mineralogy results from XRD. Similarly, the $C - H$ bond stretching at 1,420 and 2,853 cm^{-1}; and bond bending at

2,927 cm^{-1} follows the same trend, which corresponds to the variation in TOC contents from the highest (Carbonate-1) to the lowest (Carbonate-4). In addition, the carboxyl group (COOH) stretching vibrations observed at 1,798 cm^{-1} demonstrated a similar signal trend between the samples. Only the stretching frequencies of sulfonyl functional groups at 1,030 cm^{-1} and the hydroxyl functional groups at 3,622 and 3,699 cm^{-1} showed some variations. The $S = \ddot{O}$ bond demonstrated is more firmly in Carbonate-1 (the highest TOC) than Carbonate-4; Carbonate-1 > Carbonate-4 > Carbonate-3 > Carbonate-2. While the peaks of the $O - H$ bond stretching were observed as follows; Carbonate-3 > Carbonate-1 > Carbonate-4 > Carbonate-2.

4.4. Hydrogen, methane, and carbon dioxide adsorption capacities

Determining the adsorption capacity of H_2, CH_4, and CO_2 at a rock formation is crucial for understanding H_2 storage and withdrawal processes, including adsorption–desorption cycles [94]. The adsorption phenomenon occurs when the gas molecules are attached to the surface of the solid and held in its pores via physical or chemical mechanisms [65]. Van der Waals and electrostatic forces can theoretically cause physical adsorption, while chemical adsorption is driven by strong chemical bonds between the gas molecules and the rock surface [95]. Adsorption is also proportional to the applied pressure; therefore, desorption occurs when the pressure is reduced [89,96].

In general, adsorption measurements of H_2, CO_2, and CH_4 monotonically increased with increasing pressure at a constant temperature of 60 °C, as depicted in Fig. 10. Gas adsorption increases drastically under low pressures than high pressures due to its higher diffusion rate at the beginning of the adsorption process. For the H_2 adsorption, the increase initially was steep, from 0.1 to 2 MPa, and it continued to increase slightly until it reached the maximum adsorption capacity at around 9
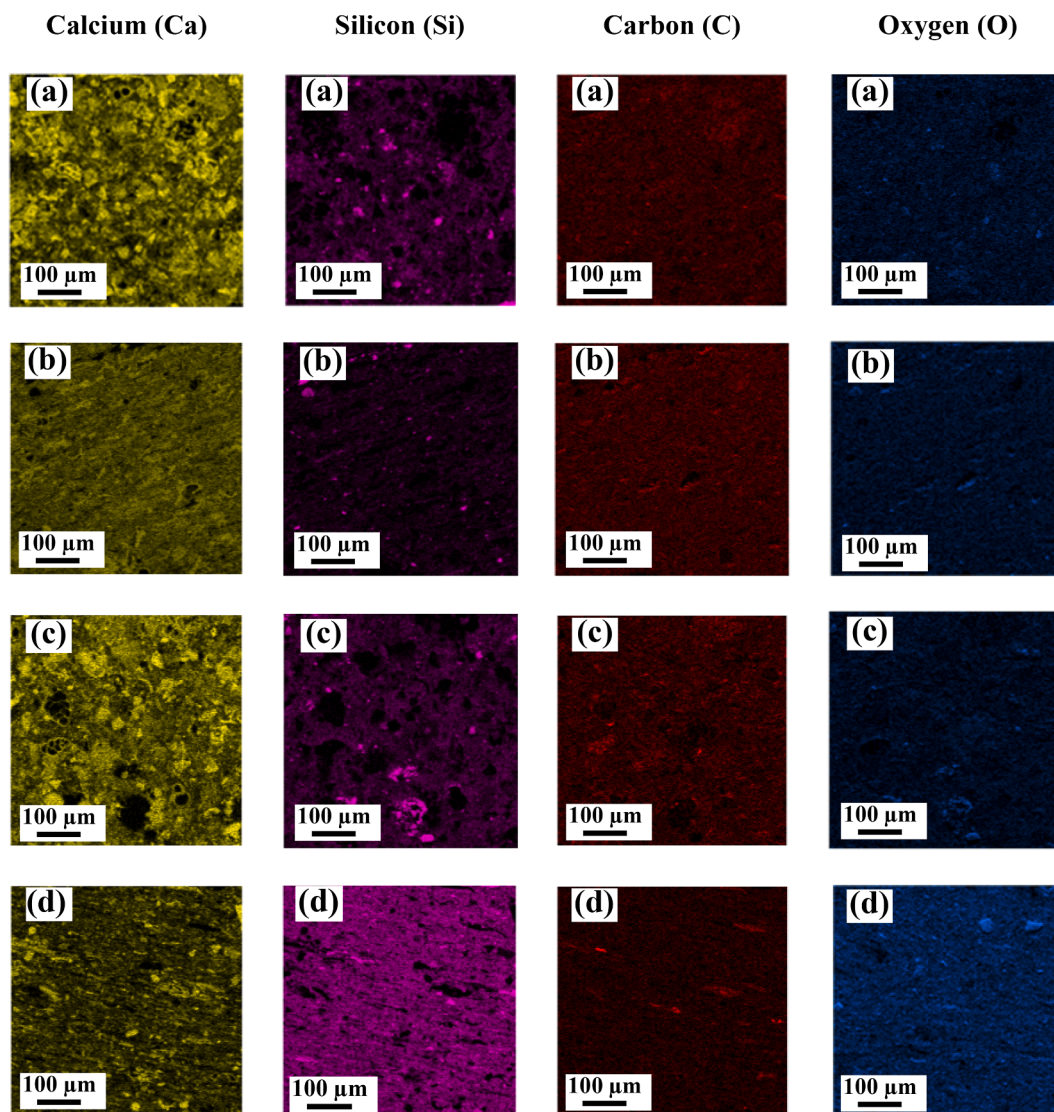
Calcium (Ca)	Silicon (Si)	Carbon (C)	Oxygen (O)

Fig. 6. Maps of the sum spectrum of dominant elements from Energy-dispersive X-ray (EDX) spectrographic on – a) Carbonate-1, b) Carbonate-2, c) Carbonate-3, and d) Carbonate-4.

MPa. Thus, only a small amount of H_2 was adsorbed at low pressure (0.001–0.008 mol of H_2/kg of rock at 0.1 MPa). The highest adsorption of 0.5 mol/kg was observed at 9 MPa for Carbonate-4 (the one with the lowest TOC), while the lowest adsorption of 0.18 mol/kg was detected for Carbonate-1 (the one with the highest TOC). Unlike N_2 adsorption that showed Type V isotherms (Fig. 5), the H_2 adsorption profiles indicate Type I isotherms and mono-layer adsorption of H_2 [26,48,97]. In addition, a marginal increase in H_2 adsorption can occur by decreasing the temperature, indicating a slight influence of the changing temperature [45,48]. Thus, H_2 adsorption was significantly increased in the studied organic-rich carbonaceous rocks (i.e., Carbonate-4) under relatively high reservoir temperature (60 °C) and high pressures (0.1 – 10.0 MPa).

Conversely, the adsorption of CH_4 and CO_2 can reach a factor of 5 and 23 times, respectively, higher than H_2 adsorption, as illustrated in Fig. 10. Below the pressure value of 2.0 MPa, the adsorption reached a very low capacity (i.e., 0.008 mol of H_2/kg at 0.1 MPa). The amount of adsorbed CO_2 at 5 MPa and 60 °C was 4.5 mol of CO_2/kg compared to 0.37 mol of H_2/kg at Carbonate-4 and 4.8 mol of CO_2/kg compared to 0.18 mol of H_2/kg at Carbonate-1. CO_2 adsorption was higher than CH_4 and H_2 because CO_2 is a Lewis acid with a higher quadrupole moment than other gases [98]. Consequently, CO_2 strongly favors calcite as it is,

a Lewis base that enormously enhances the electrostatic attraction between the CO_2 molecules and calcite [65,99,100]. Carbonates have various active functional groups, such as hydroxyl, carboxyl, and sulfonyl, which can strongly attract a guest molecule of high quadrupole moment, such as CO_2 [48]. Furthermore, the hydroxyl functional groups are more effective in enhancing CO_2 adsorption and CH_4 adsorption [45,46]. The physisorption between CO_2 and limestone was previously reported by [101], indicating very stable adsorption of CO_2 molecules on calcite at low-pressure values [43,100,102].

Additionally, TGA results in Fig. 8 confirmed that calcite content was a prime factor affecting all gases' adsorption capacity. Specifically, the decomposition of calcite refers to the content of CaO. Therefore, the deeper weight loss steps between 600 and 800 °C interpreted more enhancement in the H_2 adsorption in Carbonate-4, however higher CO_2 and CH_4 adsorption was seen in Carbonate-1 and −2 with shallow weight loss steps. Moreover, rock's surface charges can significantly influence gas adsorption [48]. Therefore, the zeta potential was measured for all the samples. The results showed relatively low zeta potential values ranging from −6.4 mV (Carbonate-4) to 0.0035 mV (Carbonate-1). All zeta potential samples were prepared using deionized water of 9.0 pH at 298 K. A low zeta potential strongly interacts with a molecule of a high quadrupole moment, such as the CO_2 quadrupole
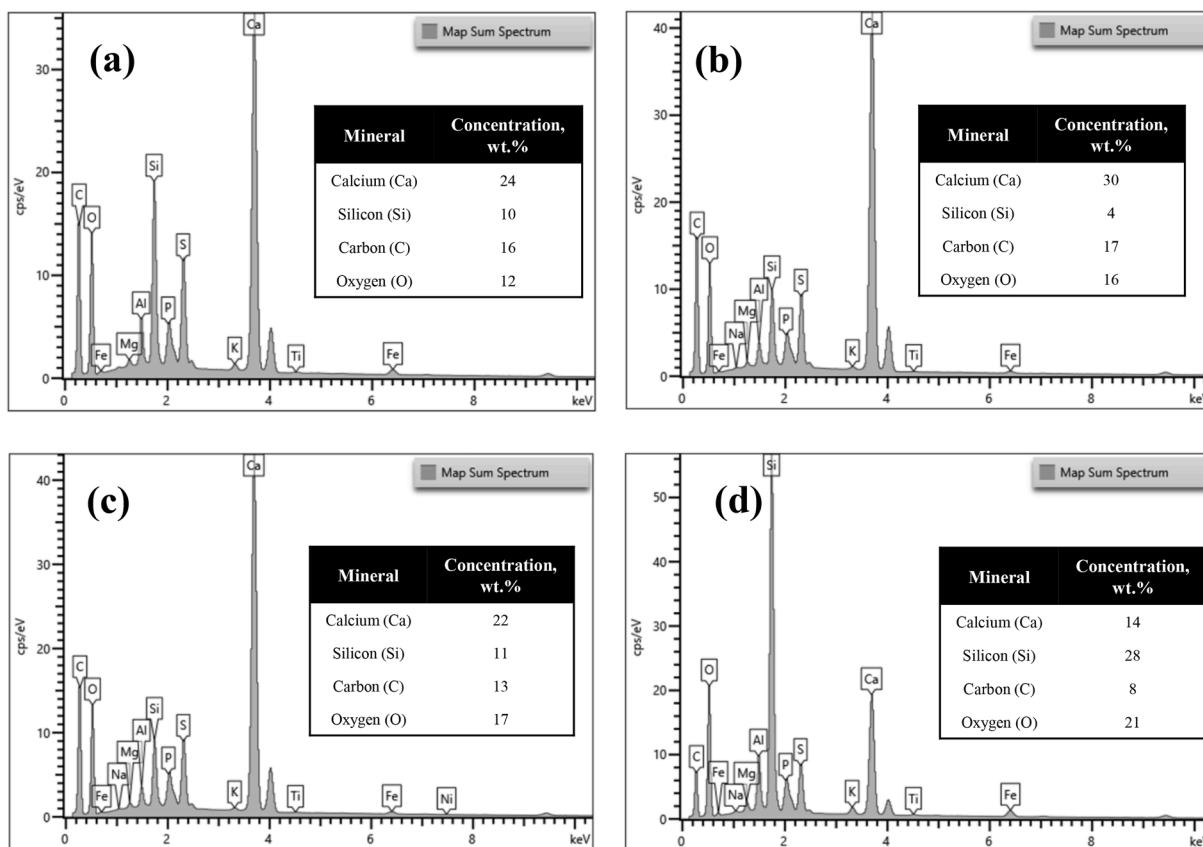
Fig. 7. Quantitative analysis of the dominant elements' composition from Energy-dispersive X-ray spectrographic (EDS) on – a) Carbonate-1, b) Carbonate-2, c) Carbonate-3, and d) Carbonate-4.
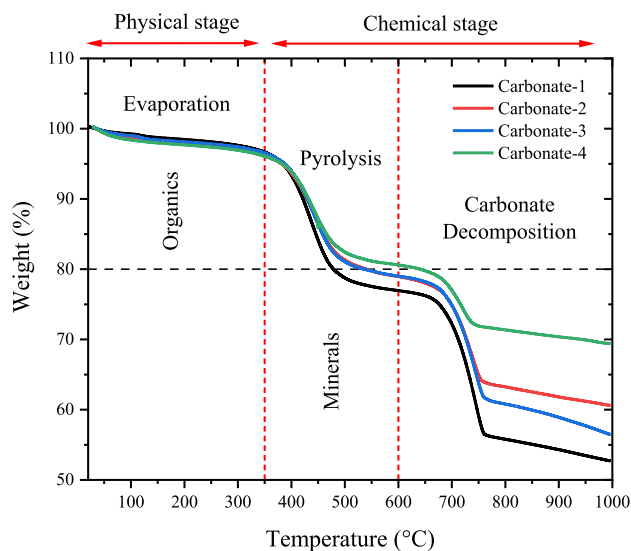

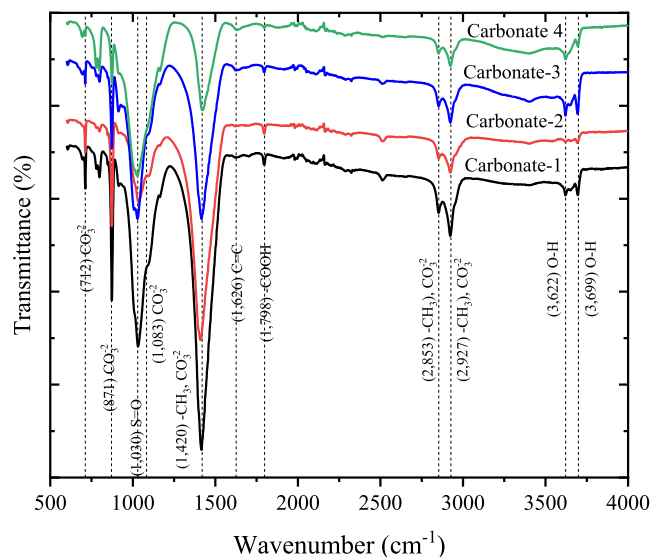**Fig. 8.** Thermo-gravimetric (TGA) analysis of the four carbonate samples.

Fig. 9. FTIR spectrum measurements for the four carbonate rock samples at different depths and varying TOC from 18% Carbonate-1 to 13% Carbonate-4.

moment of -4.3×10^{-26} esu.cm^2 [98]. The variation in the zeta potential is directly related to the calcite concentration in the carbonate samples [103,104]. On the other hand, H_2 has a smaller molecular size but a smaller positive quadrupole moment ($+0.651 \times 10^{-26}$ esu.cm^2) [98]. Thus, H_2 adsorption can be strongly enhanced when the pores are small, enriched with cavities and free from electron functional groups,

such as $C = \ddot{O}$ and $S = \ddot{O}$. In the presence of these functional groups, hydrogen molecules can behave as a weak Lewis acid (transfer electron from the functional groups of carbonate to the $\sigma^*(H_2)$ orbital) and a weak Lewis base (transfer electron from the $\sigma(H_2)$ orbital to the functional group of carbonate), which is strongly enhanced by calcite, which played a prime role as a polarizing factor enhancing the Lewis acid-base
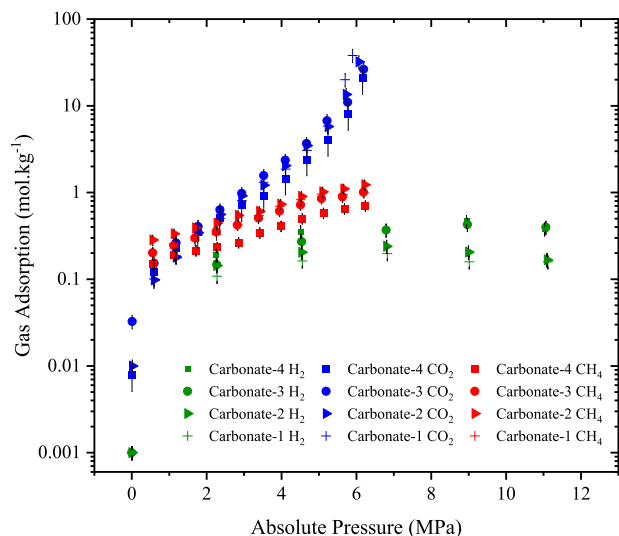
Fig. 10. Hydrogen (H_2), carbon dioxide (CO_2), and methane (CH_4) adsorption capacities in organic-rich carbonate samples as a function of pressure at 60 °C. Error bars are equivalent to 1/5. The average error values are ± 1.7 % for H_2, ±3.4 % for CO_2, and ± 2.7 % for CH_4.

interactions [45]. In addition, H_2 adsorption is likely driven by dispersive Van der Waals forces, which are substantially weaker interactions [105,106].

The FTIR spectra of the used samples were measured after each gas adsorption experiment and plotted against the FTIR of the raw samples, depicted in Fig. 11. Almost all peaks in the spectra of the samples were maintained after each gas adsorption, which was acquired at high pressure; thus, slight changes in the intensities were observed.

4.5. Gas adsorption versus total organic content (TOC)

The adsorption capacity of gas on a rock surface is highly influenced by the TOC and the thermal maturity level of the organic matter [47,49,54–57]. Hence, TOC was a critical parameter studied here by selecting varying TOC carbonate samples (i.e., from 13 % to 18 %TOC). The adsorption capacities of H_2, CO_2, and CH_4, depicted in Fig. 12, demonstrate an overall declining behavior with increasing TOC in the carbonate samples. A decline in the adsorption capacities became more significant at higher pressures, while a slight decrease was observed at lower pressures, particularly in H_2 and CH_4 at a constant temperature of 60 °C. The highest variation in adsorption (12 mol/kg) was observed for CO_2 at 5.7 MPa, indicating that lower TOC in a rock might boost the adsorption capacity.

Additionally, H_2 showed higher sensitivity to TOC than CO_2 and CH_4. A gradual decrease in H_2 adsorption with increasing TOC was also observed, consistent with the literature [13,17,36,58,59,61,107]. That is generally linked to the Hydrogen Index of the organic matter in a rock sample [108]. Moreover, the TOC in each analyzed sample corresponds to the decomposition results shown by TGA in Fig. 8 between 350 °C and 600 °C. The weight loss step of TOC (between 350 and 600 °C) confirms that the TOC is a major influencer in gas adsorption. The CO_2 and CH_4 adsorptions were higher when the step of TOC weight loss was higher, particularly in Carbonate-1 and −2; whereas the H_2 adsorption was lower, Fig. 12. Since Carbonate-2 and −3 have almost the same TOC, their degradation rates are pretty similar.

4.6. Selectivity for cushion gas and hydrogen withdrawal

Underground H_2 storage is a cyclic process of injection and
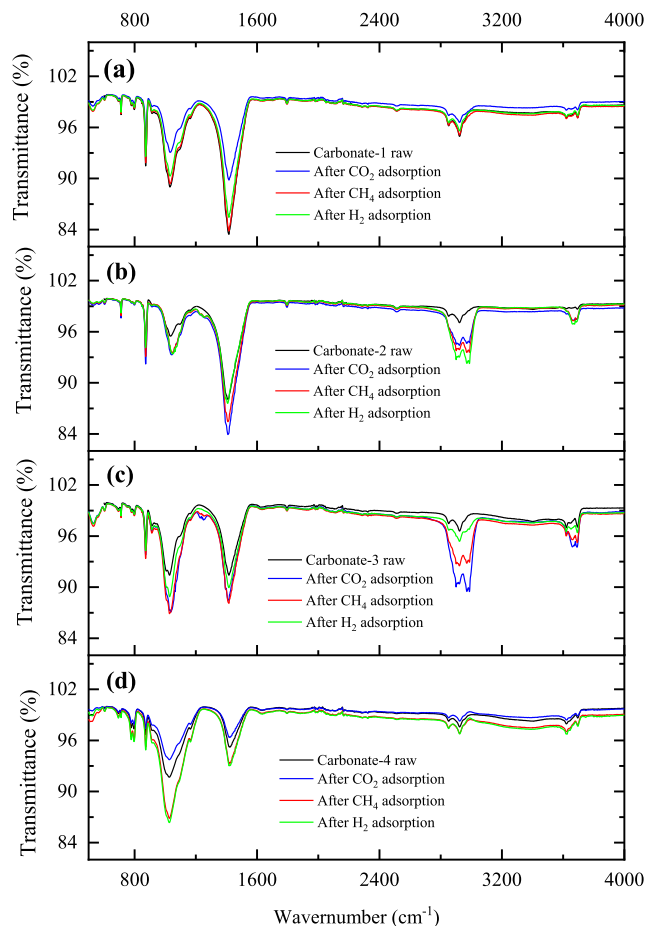
Fig. 11. Fourier-Transformed infrared spectra before and after H_2, CO_2, and CH_4 gas adsorption experiemtns –a) Carbonate-1, b) Carbonate-2, c) Carbonate-3, and d) Carbonate-4.

withdrawal of H_2 [109], where a cushion gas is utilized to maintain the pressure and provides adequate pressurization for H_2 extraction [9]. The utilization of a gas with a heavier density as a cushion gas, such as carbon dioxide or methane, has been suggested by several works in the literature [14,19,34,37]. Therefore, the selection of the cushion gas from an adsorption perspective was evaluated by measuring the adsorption of CO_2 and CH_4, as shown in Fig. 13. Both selectivities of CO_2/H_2 and CH_4/H_2 plots show nonlinear responses against pressure. The samples at low-pressure values (below 2 MPa) showed higher adsorption affinity to CH_4 than CO_2. At higher pressure values (above 2 MPa), CO_2 depicted higher adsorption capacities and consequently higher CO_2/H_2 selectivity, mainly attributed to the higher polarizability of CO_2 ($29.1x 10^{-25}$ cm^3) and due to the interactions between the CO_2 molecules with each other [110] compared to that of CH_4 (25.9×10^{-25} cm^3) and H_2 ($8 x10^{-25}$ cm^3) [111]. It is also well-established that high pressures characterize underground reservoirs. Thus, selectivity at higher pressure values is more significant [17,36,112]. By comparing the adsorption selectivity above 2 MPa pressure, CO_2/H_2 showed a sharp increase, rising from 5 to 22 times compared to H_2 adsorption, while the CH_4 adsorption ranged only from 2 to 6 times that of H_2 adsorption. Higher cushion gas adsorption was preferred during the cyclic injection and withdrawal of H_2 to ensure that the gas resides within the reservoir rock and exerts the required pressure. Hence, according to our adsorption selectivity analysis, CO_2 gas is the preferred candidate as cushion gas.
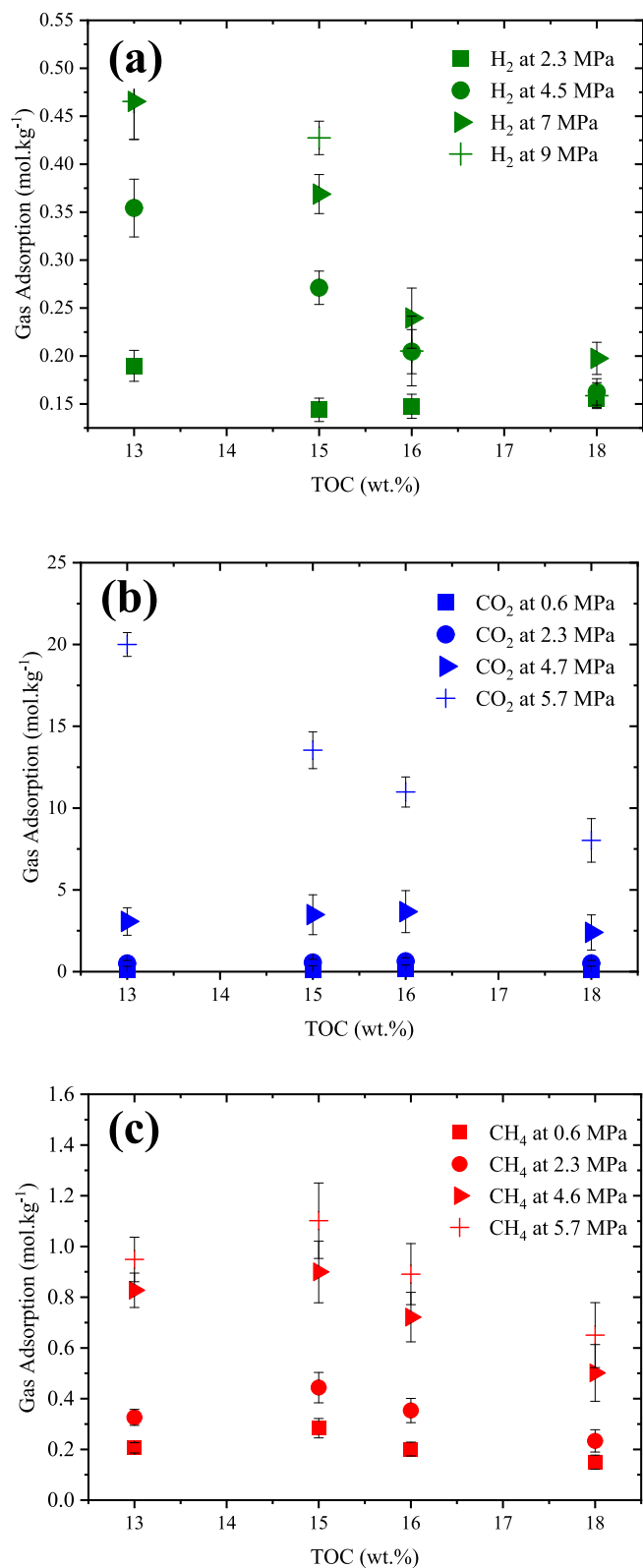
Fig. 12. Gas adsorption capacities as a function of total organic content (TOC) plotted for constant pressures and at a temperature value of 60 °C from all the analyzed organic-rich carbonate rocks for – a) Hydrogen (H_2), b) Carbon dioxide (CO_2), and c) Methane (CH_4). Error bars are equivalent to 1/5. The average error values are ± 1.7 % for H_2, ±3.4 % for CO_2, and ± 2.7 % for CH_4.
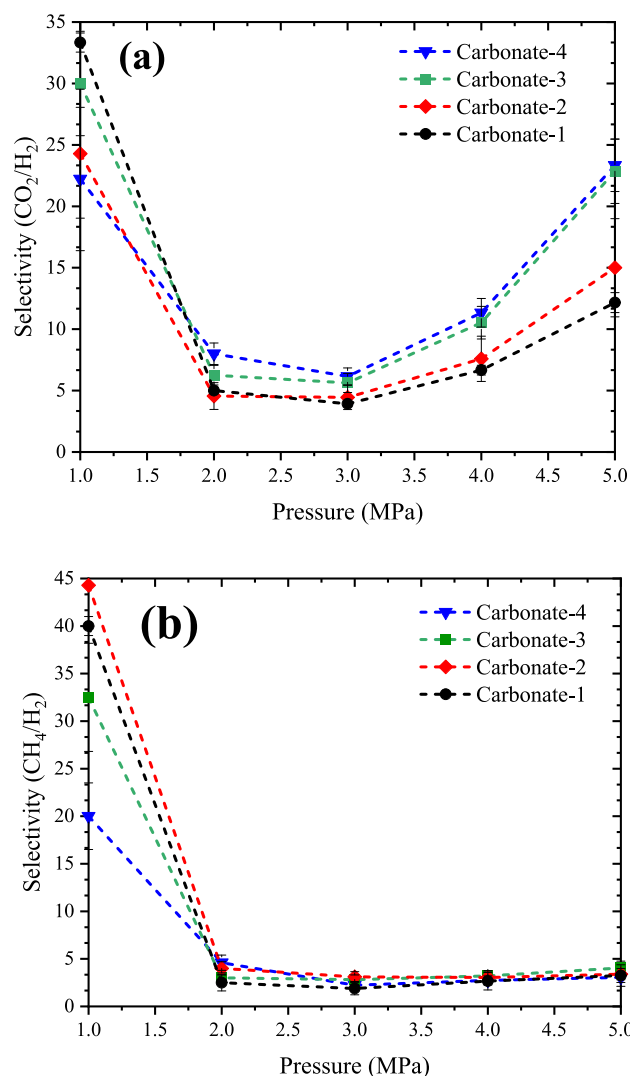
Fig. 13. Plotting of gas adsorption selectivity as a function of pressure and at a temperature value of 60 °C for the four carbonaceous samples - a) CO_2/H_2 and b) CH_4/H_2. The shaded area behind the data points represents the error bar. The average error values are ± 1.7 % for H_2, ±3.4 % for CO_2, and ± 2.7 % for CH_4.

5. Conclusion

Underground hydrogen storage (UHS) is essential for its significant storage capacity, low operational cost, and firm natural security [16,113,114]. However, the presence of organic residuals can significantly influence the H_2 storage process and cushion gas efficiency [41,115,116]. Therefore, this work systematically studied the adsorption capacities of H_2, CO_2, and CH_4 using actual organic-rich source rocks (with high carbonate content) for the first time and investigated the influence of different TOC on H_2 geo-storage and retrieval.

Initially, various analytical methods (energy-dispersive X-ray mapping, scanning electron microscopy, X-ray diffraction, Fourier-transformed infrared spectroscopy, zeta-potential, thermo-gravimetric and BET analysis) were used to determine the elemental composition, bulk mineralogy, surface functional groups, surface charge, thermal decomposition, and pore size distribution. After that, H_2, CO_2, and CH_4 adsorption isotherms were measured at the reservoir's temperature (60 °C) and wide range of pressures (0.1 – 10.0 MPa).

The retrieval of the stored H_2 was investigated in this work, where the selectivity of CO_2 and CH_4 over H_2 were also examined. Over the studied range of pressures, H_2 adsorption showed a significantly

decreasing trend with increasing TOC. The lowest TOC (Carbonate-4) demonstrated the highest H$_2$ adsorption and the highest selectivity for CO$_2$ over H$_2$. The calcite, carboxyl, and sulfonyl functional groups were the affective factors in enhancing H$_2$ adsorption in carbonate samples. In addition, the calcite with hydroxyl groups significantly improved CO$_2$ adsorption. Based on the adsorption criterion, CO$_2$ was considered a superior cushion gas to CH$_4$ for its higher adsorption capacity. Moreover, it was also indicated that carbonate rocks are feasible options for storing and extracting H$_2$ for high seasonal demands. This study provides essential data for H$_2$ storage issues in high TOC carbonate formations and thus aids in the industrial implementation of a hydrogen supply chain.

CRediT authorship contribution statement

Amer Alanazi: Conceptualization, Methodology, Investigation, Data curation, Software, Writing – original draft. **Hussein Rasool Abid:** Methodology, Investigation, Data curation. **Muhammad Usman:** Conceptualization, Validation, Formal analysis, Writing – review & editing. **Muhammad Ali:** Formal analysis, Validation, Writing – review & editing. **Alireza Keshavarz:** Visualization, Writing – review & editing. **Volker Vahrenkamp:** Visualization, Writing – review & editing. **Stefan Iglauer:** Validation, Resources, Writing – review & editing, Supervision. **Hussein Hoteit:** Conceptualization, Validation, Resources, Writing – review & editing, Project administration, Supervision.

Declaration of Competing Interest

The authors declare that they have no known competing financial interests or personal relationships that could have appeared to influence the work reported in this paper.

Data availability

Data will be made available on request.

Acknowledgments

Appendix A. Supplementary data

Supplementary data to this article can be found online at https://doi.org/10.1016/j.fuel.2023.128362.

References

[1] Hanley ES, Deane JP, Gallachóir BPÓ. The role of hydrogen in low carbon energy futures–A review of existing perspectives. Renew Sustain Energy Rev 2018;82: 3027–45.

[2] Tarkowski R, Czapowski G. Salt domes in Poland – Potential sites for hydrogen storage in caverns. Int J Hydrogen Energy 2018;43(46):21414–27.

[3] Tarkowski R. Underground hydrogen storage: Characteristics and prospects. Renew Sustain Energy Rev 2019;105:86–94.

[4] IEA, Renewables 2019 – Analysis - IEA, Int. Energy Agency. (2019).

[5] McPherson M, Johnson N, Strubegger M. The role of electricity storage and hydrogen technologies in enabling global low-carbon energy transitions. Appl Energy 2018;216:649–61.

[6] Chen H, Song J, Zhao J. Synergies between power and hydrogen carriers using fuel-cell hybrid electrical vehicle and power-to-gas storage as new coupling points. Energy Convers Manag 2021;246:114670.

[7] Berta M, Dethlefsen F, Ebert M, Schäfer D, Dahmke A. Geochemical Effects of Millimolar Hydrogen Concentrations in Groundwater: An Experimental Study in the Context of Subsurface Hydrogen Storage. Environ Sci Technol 2018;52: 4937–49. https://doi.org/10.1021/ACS.EST.7B05467/ASSET/IMAGES/LARGE/ES-2017-05467W_0005.JPEG.

[8] Flesch S, Pudlo D, Albrecht D, Jacob A, Enzmann F. Hydrogen underground storage—Petrographic and petrophysical variations in reservoir sandstones from laboratory experiments under simulated reservoir conditions. Int J Hydrogen Energy 2018;43:20822–35. https://doi.org/10.1016/J.IJHYDENE.2018.09.112.

[9] Heinemann N, Alcalde J, Miocic JM, Hangx SJT, Kallmeyer J, Ostertag-Henning C, et al. Enabling large-scale hydrogen storage in porous media – the scientific challenges. Energy Environ Sci 2021;14:853–64. https://doi.org/10.1039/D0EE03536J.

[10] Lord AS, Kobos PH, Borns DJ. Geologic storage of hydrogen: Scaling up to meet city transportation demands. Int J Hydrogen Energy 2014;39:15570–82. https://doi.org/10.1016/J.IJHYDENE.2014.07.121.

[11] Yekta AE, Manceau J-C-C, Gaboreau S, Pichavant M, Audigane P. Determination of Hydrogen-Water Relative Permeability and Capillary Pressure in Sandstone: Application to Underground Hydrogen Injection in Sedimentary Formations. Transp Porous Media 2018;122:333–56. https://doi.org/10.1007/S11242-018-1004-7/FIGURES/12.

[12] Zhang F, Zhao P, Niu M, Maddy J. The survey of key technologies in hydrogen energy storage. Int J Hydrogen Energy 2016;41:14535–52. https://doi.org/10.1016/J.IJHYDENE.2016.05.293.

[13] Ali M, Yekeen N, Alanazi A, Keshavarz A, Iglauer S, Finkbeiner T, et al. Saudi Arabian basalt/CO2/brine wettability: Implications for CO2 geo-storage. J Energy Storage 2023;62:106921. https://doi.org/10.1016/J.EST.2023.106921.

[14] Hashemi L, Boon M, Glerum W, Farajzadeh R, Hajibeygi H. A comparative study for H2-CH4 mixture wettability in sandstone porous rocks relevant to underground hydrogen storage. Adv Water Resour 2022;163:104165. https://doi.org/10.1016/J.ADVWATRES.2022.104165.

[15] Ali M, Pan B, Yekeen N, Al-Anssari S, Al-Anazi A, Keshavarz A, et al. Assessment of wettability and rock-fluid interfacial tension of caprock: Implications for hydrogen and carbon dioxide geo-storage. Int J Hydrogen Energy 2022;47(30): 14104–20.

[16] S. Iglauer M. Ali A. Keshavarz Hydrogen Wettability of Sandstone Reservoirs: Implications for Hydrogen Geo-Storage Geophys. Res. Lett. 48 2021 e2020GL090814 10.1029/2020GL090814.

[17] Alanazi A, Bawazeer S, Ali M, Keshavarz A, Hoteit H. Thermodynamic Modeling of Hydrogen-Water Systems with Gas Impurity at Various Conditions Using Cubic and PC-SAFT Equations of State. Energy Convers Manag 2022;X:100257. https://doi.org/10.1016/J.ECMX.2022.100257.

[18] Ozarslan A. Large-scale hydrogen energy storage in salt caverns. Int J Hydrogen Energy 2012;37(19):14265–77.

[19] Zivar D, Kumar S, Foroozesh J. Underground hydrogen storage: A comprehensive review. Int J Hydrogen Energy 2021;46(45):23436–62.

[20] Pan B, Yin X, Ju Y, Iglauer S. Underground hydrogen storage: Influencing parameters and future outlook. Adv Colloid Interface Sci 2021;294:102473.

[21] Hashemi L, Glerum W, Farajzadeh R, Hajibeygi H. Contact angle measurement for hydrogen/brine/sandstone system using captive-bubble method relevant for underground hydrogen storage. Adv Water Resour 2021;154:103964. https://doi.org/10.1016/J.ADVWATRES.2021.103964.

[22] Hosseini M, Fahimpour J, Ali M, Keshavarz A, Iglauer S. Hydrogen wettability of carbonate formations: Implications for hydrogen geo-storage. J Colloid Interface Sci 2022;614:256–66. https://doi.org/10.1016/J.JCIS.2022.01.068.

[23] Ali M, Yekeen N, Pal N, Keshavarz A, Iglauer S, Hoteit H. Influence of organic molecules on wetting characteristics of mica/H2/brine systems: Implications for hydrogen structural trapping capacities. J Colloid Interface Sci 2022;608: 1739–49. https://doi.org/10.1016/J.JCIS.2021.10.080.

[24] Al-Areeq NM. Petroleum Source Rocks Characterization and Hydrocarbon Generation. Recent Insights Pet Sci Eng 2018. https://doi.org/10.5772/INTECHOPEN.70092.

[25] Baur FUM, Katz BJ, Gaus G. Gas sorption in source rocks – A short discussion. Int J Coal Geol 2020;219:103372. https://doi.org/10.1016/J.COAL.2019.103372.

[26] Abid HR, Iglauer S, Al-Yaseri A, Keshavarz A. Drastic enhancement of CO2 adsorption capacity by negatively charged sub-bituminous coal. Energy 2021; 233:120924.

[27] S. Iglauer H. Akhondzadeh H. Abid A. Paluszny A. Keshavarz M. Ali et al. Hydrogen Flooding of a Coal Core: Effect on Coal Swelling Geophys. Res. Lett. 49 2022 e2021GL096873 10.1029/2021GL096873.

[28] Buzek F, Lnenickova Z. Temperature programmed desorption of coal gases - Chemical and carbon isotope composition. Fuel 2010;89(7):1514–24.

[29] Yekeen N, Al-Yaseri A, Negash BM, Ali M, Giwelli A, Esteban L, et al. Clay-hydrogen and clay-cushion gas interfacial tensions: Implications for hydrogen storage. Int J Hydrogen Energy 2022;47:19155–67. https://doi.org/10.1016/J.IJHYDENE.2022.04.103.

[30] Taylor J, Alderson J, Kalyanam K, Lyle A, Phillips L. Technical and economic assessment of methods for the storage of large quantities of hydrogen. Int J Hydrogen Energy 1986;11(1):5–22.

[31] Al-Yaseri A, Wolff-Boenisch D, Fauziah CA, Iglauer S. Hydrogen wettability of clays: Implications for underground hydrogen storage. Int J Hydrogen Energy 2021;46(69):34356–61.

[32] Oldenburg CM, Pan L. Utilization of CO2 as cushion gas for porous media compressed air energy storage. Greenh Gases Sci Technol 2013;3(2):124–35.

[33] Oldenburg CM. Carbon dioxide as cushion gas for natural gas storage. Energy Fuel 2003;17:240–6. https://doi.org/10.1021/ef020162b.

[34] Ma J, Li Qi, Kempka T, Kühn M. Hydromechanical response and impact of gas mixing behavior in subsurface CH4 Storage with CO2-based cushion gas. Energy Fuel 2019;33(7):6527–41.

[35] Ibrahim AF, Abdelgawad KZ, Al-Anazi A, Al Hamad JS. Effect of Crude Oil Properties on the Interfacial Tension of Crude Oil/CO2 Under HPHT Conditions. Arab J Sci Eng 2022. https://doi.org/10.1007/S13369-022-07291-6.

[36] Alanazi A, Ali M, Bawazeer S, Yekeen N, Hoteit H. Evaluation of cubic, PC-SAFT, and GERG2008 equations of state for accurate calculations of thermophysical properties of hydrogen-blend mixtures. Energy Rep 2022;8:13876–99. https://doi.org/10.1016/J.EGYR.2022.10.257.

[37] Mokhatab S, Poe WA, Mak JY. Handbook of natural gas transmission and processing: Principles and practices. Handb Nat Gas Transm Process Princ Pract 2018:1–826. https://doi.org/10.1016/C2017-0-03889-2.

[38] Abdulelah H, Al-Yaseri A, Ali M, Giwelli A, Negash BM, Sarmadivaleh M. CO2/ Basalt's interfacial tension and wettability directly from gas density: Implications for Carbon Geo-sequestration. J Pet Sci Eng 2021;204:108683.

[39] Al-Yaseri A, Ali M, Ali M, Taheri R, Wolff-Boenisch D. Western Australia basalt-CO2-brine wettability at geo-storage conditions. J Colloid Interface Sci 2021;603: 165–71. https://doi.org/10.1016/J.JCIS.2021.06.078.

[40] Iglauer S, Pentland CH, Busch A. CO2 wettability of seal and reservoir rocks and the implications for carbon geo-sequestration. Water Resour Res 2015;51:729–74. https://doi.org/10.1002/2014WR015553.

[41] Ali M, Aftab A, Arain Z-U-A, Al-Yaseri A, Roshan H, Saeedi A, et al. Influence of Organic Acid Concentration on Wettability Alteration of Cap-Rock: Implications for CO2Trapping/Storage. ACS Appl Mater Interfaces 2020;12(35):39850–8.

[42] Arif M, Rasool Abid H, Keshavarz A, Jones F, Iglauer S. Hydrogen storage potential of coals as a function of pressure, temperature, and rank. J Colloid Interface Sci 2022;620:86–93. https://doi.org/10.1016/J.JCIS.2022.03.138.

[43] Ottiger S, Pini R, Storti G, Mazzotti M. Measuring and modeling the competitive adsorption of CO2, CH4, and N2 on a dry coal. Langmuir 2008;24(17):9531–40.

[44] Keshavarz A, Abid H, Ali M, Iglauer S. Hydrogen diffusion in coal: Implications for hydrogen geo-storage. J Colloid Interface Sci 2022;608:1457–62.

[45] Rasool Abid H, Keshavarz A, Lercher J, Iglauer S. Promising Material for Large-Scale H2 Storage and Efficient H2-CO2 Separation. Sep Purif Technol 2022;298: 121542.

[46] Abid H, Yekeen N, Al-Yaseri A, Keshavarz A, Iglauer S. The impact of humic acid on hydrogen adsorptive capacity of eagle ford shale: Implications for underground hydrogen storage. J Energy Storage 2022;55:105615. https://doi.org/10.1016/J.EST.2022.105615.

[47] Shabani M, Moallemi SA, Krooss BM, Amann-Hildenbrand A, Zamani-Pozveh Z, Ghalavand H, et al. Methane sorption and storage characteristics of organic-rich carbonaceous rocks, Lurestan province, southwest Iran. Int J Coal Geol 2018;186: 51–64. https://doi.org/10.1016/J.COAL.2017.12.005.

[48] S. Iglauer H. Abid A. Al-Yaseri A. Keshavarz Hydrogen Adsorption on Sub-Bituminous Coal: Implications for Hydrogen Geo-Storage Geophys. Res. Lett. 48 2021 e2021GL092976 10.1029/2021GL092976.

[49] Bakshi T, Vishal V. A Review on the Role of Organic Matter in Gas Adsorption in Shale. Energy Fuel 2021;35:15249–64. https://doi.org/10.1021/ACS.ENERGYFUELS.1C01631.

[50] Liu Y, Wilcox J. Molecular simulation of CO2 adsorption in micro- and mesoporous carbons with surface heterogeneity. Int J Coal Geol 2012;104:83–95. https://doi.org/10.1016/J.COAL.2012.04.007.

[51] Chen G, Zhang J, Lu S, Pervukhina M, Liu K, Xue Q, et al. Adsorption Behavior of Hydrocarbon on Illite. Energy Fuel 2016;30:9114–21. https://doi.org/10.1021/ACS.ENERGYFUELS.6B01777/ASSET/IMAGES/LARGE/EF-2016-01777R_0005.JPEG.

[52] Mosher K, He J, Liu Y, Rupp E, Wilcox J. Molecular simulation of methane adsorption in micro- and mesoporous carbons with applications to coal and gas shale systems. Int J Coal Geol 2013;109–110:36–44. https://doi.org/10.1016/J.COAL.2013.01.001.

[53] Yang F, Ning Z, Zhang R, Zhao H, Krooss BM. Investigations on the methane sorption capacity of marine shales from Sichuan Basin, China. Int J Coal Geol 2015;146:104–17. https://doi.org/10.1016/J.COAL.2015.05.009.

[54] Zhang T, Ellis GS, Ruppel SC, Milliken K, Yang R. Effect of organic-matter type and thermal maturity on methane adsorption in shale-gas systems. Org Geochem 2012;47:120–31.

[55] Huang H, Li R, Lyu Z, Cheng Y, Zhao B, Jiang Z, et al. Comparative study of methane adsorption of Middle-Upper Ordovician marine shales in the western Ordos Basin, NW China: Insights into impacts of moisture on thermodynamics and kinetics of adsorption. Chem Eng J 2022;446:137411.

[56] Gasparik M, Bertier P, Gensterblum Y, Ghanizadeh A, Krooss BM, Littke R. Geological controls on the methane storage capacity in organic-rich shales. Int J Coal Geol 2014;123:34–51.

[57] Ji L, Zhang T, Milliken KL, Qu J, Zhang X. Experimental investigation of main controls to methane adsorption in clay-rich rocks. Appl Geochemistry 2012;27: 2533–45. https://doi.org/10.1016/j.apgeochem.2012.08.027.

[58] Alanazi A, Yekeen N, Ali M, Ali M, Abu-Mahfouz IS, Keshavarz A, et al. Influence of organics and gas mixing on hydrogen/brine and methane/brine wettability using Jordanian oil shale rocks: Implications for hydrogen geological storage. J Energy Storage 2023;62:106865.

[59] Shar AM, Ali M, Bhutto DK, Alanazi A, Akhondzadeh H, Keshavarz A, et al. Cryogenic Liquid Nitrogen Fracking Effects on Petro-Physical and Morphological

Characteristics of the Sembar Shale Gas Formation in the Lower Indus Basin, Pakistan. Energy Fuel 2022. https://doi.org/10.1021/ACS.ENERGYFUELS.2C02257/ASSET/IMAGES/LARGE/EF2C02257_0008.JPEG.

[60] A. Alanazi, M. Al Malallah, M. Mowafi, W. Badeghaish, H. Hoteit, A. Al-Yaseri, J. Al-Hamad, Hydrogen Wettability Measurement of Saudi Basaltic Rocks at Underground Storage Conditions, All Days. (2022). https://doi.org/10.56952/IGS-2022-110.

[61] A. Alanazi, M. Ali, M. Mowafi, H. Hoteit, Effect of Organics and Nanofluids on Capillary-Sealing Efficiency of Caprock for Hydrogen and Carbon-Dioxide Geological Storage, All Days. (2022). https://doi.org/10.56952/IGS-2022-009.

[62] Arif M, Zhang Y, Iglauer S. Shale wettability: Data sets, challenges, and outlook. Energy Fuel 2021;35:2965–80.

[63] Arif M, Lebedev M, Barifcani A, Iglauer S. Influence of shale-total organic content on CO2 geo-storage potential. Geophys Res Lett 2017;44:8769–75. https://doi.org/10.1002/2017GL073532.

[64] Iglauer S, Al-Yaseri AZ, Wolff-Boenisch D. Basalt-CO2-brine wettability at storage conditions in basaltic formations. Int J Greenh Gas Control 2020;102:103148. https://doi.org/10.1016/J.IJGGC.2020.103148.

[65] Eliebid M, Mahmoud M, Shawabkeh R, Elkatatny S, Hussein IA. Effect of CO2 adsorption on enhanced natural gas recovery and sequestration in carbonate reservoirs. J Nat Gas Sci Eng 2018;55:575–84. https://doi.org/10.1016/J.JNGSE.2017.04.019.

[66] Mahmoud M. Effect of Gas Adsorption on the Estimation of Gas in Place (GIP) in Conventional and Unconventional Reservoirs. Arab J Sci Eng 2019;44(6): 6205–14.

[67] Abed AM, Amireh BS. Petrography and geochemistry of some Jordanian oil shales from north Jordan. J Pet Geol 1983;5(3):261–74.

[68] Mahdawi HS, Mustafa HA. Petrography and Geochemistry of the Upper Cretaceous-Lower Tertiary Oil Shale, NW - Jordan. Basic Sci Eng 2007;16: 293–318.

[69] Abu-Hamatteh ZSH, Al-Shawabkeh AF. An overview of the Jordanian oil shale: Its chemical and geologic characteristics, exploration, reserves and feasibility for oil and cement production. Cent Eur Geol 2008;51(4):379–95.

[70] K.M. Ibrahim S. Aljurf H.A. Rahman C. Gülamber Exploration and evaluation of oil shale resources from attarat area, central Jordan IMCET 2019 - Proc. 26th Int. Min. Congr. Exhib 2019 Turkey.

[71] Hussein MA, Alquudah M, Podlaha OG. Ichnofabrics of Eocene oil shales from central Jordan and their use for paleoenvironmental reconstructions. GeoArabia 2014;19(1):85–112.

[72] Ahmad F, Baioumy H, Farouk S, Al-Kahtany K, El-Sorogy A, Kirk J, et al. Geochemistry and stable isotopes of the upper Campanian–lower Maastrichtian phosphorite-bearing sequence, Central Jordan: Implications for their age, origin, and diagenesis. Geol J 2020;55(6):4453–68.

[73] Abu-Mahfouz IS, Cartwright JA, Idiz E, Hooker JN, Robinson S, van den Boorn S. Genesis and role of bitumen in fracture development during early catagenesis. Pet Geosci 2019;25(4):371–88.

[74] Abu-Mahfouz IS, Cartwright J, Idiz E, Hooker JN, Robinson SA. Silica diagenesis promotes early primary hydrocarbon migration. Geology 2020;48(5):483–7.

[75] Alquudah M, Ali Hussein M, van den Boorn S, Podlaha OG, Mutterlose J. Biostratigraphy and depositional setting of Maastrichtian - Eocene oil shales from Jordan. Mar Pet Geol 2015;60. https://doi.org/10.1016/j.marpetgeo.2014.07.025.

[76] Martin AZ. Late Permian to Holocene paleofacies evolution of the Arabian Plate and its hydrocarbon occurrences. GeoArabia 2001;6(3):445–504.

[77] Powell JH, Moh'd BK. Evolution of Cretaceous to Eocene alluvial and carbonate platform sequences in central and south Jordan. GeoArabia 2011;16(4):29–82.

[78] Hakimi MH, Abdullah WH, Alquudah M, Makeen YM, Mustapha KA. Organic geochemical and petrographic characteristics of the oil shales in the Lajjun area, Central Jordan: Origin of organic matter input and preservation conditions. Fuel 2016;181:34–45.

[79] Behar F, Beaumont V, De HL, Penteado B. Rock-Eval 6 Technology: Performances and Developments. Oil Gas Sci Technol 2001;56. https://doi.org/10.2516/ogst:2001013.

[80] Carvajal-Ortiz H, Gentzis T, Ostadhassan M. Sulfur Differentiation in Organic-Rich Shales and Carbonates via Open-System Programmed Pyrolysis and Oxidation: Insights into Fluid Souring and H2S Production in the Bakken Shale, United States. Energy Fuel 2021;35:12030–44.

[81] Sayyouh MH, Al-Blehed MS. Applications of the Enhanced Recovery Methods to Saudi Oil Fields. J King Saud Univ - Eng Sci 1992;4:95–103. https://doi.org/10.1016/S1018-3639(18)30558-0.

[82] Saudi A, Swarieh A. Geothermal Energy Resources in Jordan, Country Update Report. Proc World Geotherm Congr 2005:24–9.

[83] Liu Yu, Zhu Y, Liu S, Li Wu, Tang X. Temperature effect on gas adsorption capacity in different sized pores of coal: Experiment and numerical modeling. J Pet Sci Eng 2018;165:821–30.

[84] Heller R, Zoback M. Adsorption of methane and carbon dioxide on gas shale and pure mineral samples. J Unconv Oil Gas Resour 2014;8:14–24. https://doi.org/10.1016/J.JUOGR.2014.06.001.

[85] Yin J, Kang X, Qin C, Feng B, Veeraragavan A, Saulov D. Modeling of CaCO3 decomposition under CO2/H2O atmosphere in calcium looping processes. Fuel Process Technol 2014;125:125–38. https://doi.org/10.1016/J.FUPROC.2014.03.036.

[86] Keshavarz A, Sakurovs R, Grigore M, Sayyafzadeh M. Effect of maceral composition and coal rank on gas diffusion in Australian coals. Int J Coal Geol 2017;173:65–75. https://doi.org/10.1016/J.COAL.2017.02.005.

[87] R.J. Dunham, Classification of Carbonate Rocks According to Depositional Textures, in: Classif. Carbonate Rocks–A Symp., 1962.

[88] Rouquerol J, Avnir D, Fairbridge CW, Everett DH, Haynes JM, Pernicone N, et al. Recommendations for the characterization of porous solids (Technical Report). Pure Appl Chem 1994;66:1739–58. https://doi.org/10.1351/PAC199466081739/MACHINEREADABLECITATION/RIS.

[89] Sing KSW, Everett DH, Haul RAW, Moscou L, Pierotti RA, Rouquerol J, et al. Reporting Physisorption Data for Gas/Solid Systems with Special Reference to the Determination of Surface Area and Porosity. Pure Appl Chem 1985;57:603–19. https://doi.org/10.1351/PAC198557040603/MACHINEREADABLECITATION/RIS.

[90] Garcia-Diego C, Cuellar J. Synthesis of macroporous poly(styrene-co-divinylbenzene) microparticles using n-Heptane as the porogen: Quantitative effects of the DVB concentration and the monomeric fraction on their structural characteristics. Ind Eng Chem Res 2005;44:8237–47. https://doi.org/10.1021/IE050091E/ASSET/IMAGES/MEDIUM/IE050091EE00006.GIF.

[91] Andersson L, Herring A, Schlüter S, Wildenschild D. Defining a novel pore-body to pore-throat "Morphological Aspect Ratio" that scales with residual non-wetting phase capillary trapping in porous media. Adv Water Resour 2018;122:251–62.

[92] Rodriguez-Blanco JD, Shaw S, Benning LG. The kinetics and mechanisms of amorphous calcium carbonate (ACC) crystallization to calcite, viavaterite. Nanoscale 2011;3:265–71. https://doi.org/10.1039/C0NR00589D.

[93] Andersen FA, Brečević L, Beuter G, Dell'Amico DB, Calderazzo F, Bjerrum NJ, et al. Infrared spectra of amorphous and crystalline calcium carbonate. Acta Chem Scand 1991;45:1018–24.

[94] Tajnik T, Bogataj LK, Jurač E, Lasnik CR, Likar J, Debelak B. Investigation of adsorption properties of geological materials for CO2 storage. Int J Energy Res 2013;37:952–8. https://doi.org/10.1002/ER.2901.

[95] F.G. Helfferich, Principles of adsorption & adsorption processes, by D. M. Ruthven, John Wiley & Sons, 1984, xxiv + 433 pp, AIChE J. 31 (1985) 523–524. https://doi.org/10.1002/AIC.690310335.

[96] Brunauer S, Deming LS, Deming WE, Teller E. On a Theory of the van der Waals Adsorption of Gases. J Am Chem Soc 1940;62(7):1723–32.

[97] Gil A, Massinon A, Grange P. Analysis and comparison of the microporosity in Al-, Zr- and Ti-pillared clays. Microporous Mater 1995;4(5):369–78.

[98] Buckingham AD, Disch RL, Dunmur DA. The quadrupole moments of some simple molecules. J Am Chem Soc 1968;90(12):3104–7.

[99] Zhao H, Yan W, Bian Z, Hu J, Liu H. Investigation of Mg modified mesoporous silicas and their CO 2 adsorption capacities. Solid State Sci 2012;14(2):250–7.

[100] Van Cuong P, Kuznetsova T, Kvamme B, Jensen B. Adsorption energy and stability of H2O and CO2 on calcite effect by short-range force field parameters and temperature. Carbon N Y 2012;1.

[101] van Bergen F, Spiers C, Floor G, Bots P. Strain development in unconfined coals exposed to CO2, CH4 and Ar: Effect of moisture. Int J Coal Geol 2009;77(1-2):43–53.

[102] Abunowara M, Bustam MA, Sufian S, Eldemerdash U. Description of Carbon Dioxide Adsorption and Desorption onto Malaysian Coals under Subcritical Condition. Procedia Eng 2016;148:600–8.

[103] Moulin P, Roques H. Zeta potential measurement of calcium carbonate. J Colloid Interface Sci 2003;261:115–26. https://doi.org/10.1016/S0021-9797(03)00057-2.

[104] Al Mahrouqi D, Vinogradov J, Jackson MD. Zeta potential of artificial and natural calcite in aqueous solution. Adv Colloid Interface Sci 2017;240:60–76.

[105] Keil RG, Mayer LM. Mineral Matrices and Organic Matter. Treatise Geochemistry Second Ed 2014;12:337–59. https://doi.org/10.1016/B978-0-08-095975-7.01024-X.

[106] Kleber M, Eusterhues K, Keiluweit M, Mikutta C, Mikutta R, Nico PS. Mineral-Organic Associations: Formation, Properties, and Relevance in Soil Environments. Adv Agron 2015;130:1–140. https://doi.org/10.1016/BS.AGRON.2014.10.005.

[107] Dong T, Harris NB, McMillan JM, Twemlow CE, Nassichuk BR, Bish DL. A model for porosity evolution in shale reservoirs: An example from the Upper Devonian Duvernay Formation, Western Canada Sedimentary Basin. Am Assoc Pet Geol Bull 2019;103:1017–44. https://doi.org/10.1306/10261817272.

[108] El Nady MM, Hussein SA, Sharaf LM, Ghanem MF. Quantity, thermal maturity of organic matter and relation to prospective source rock horizons in Tut-1x well, North Western Desert, Egypt. Energy Sources Part A 2016;38(21):3187–94.

[109] Amid A, Mignard D, Wilkinson M. Seasonal storage of hydrogen in a depleted natural gas reservoir. Int J Hydrogen Energy 2016;41:5549–58. https://doi.org/10.1016/j.ijhydene.2016.02.036.

[110] Walton KS, Abney MB, Douglas LeVan M. CO2 adsorption in y and X zeolites modified by alkali metal cation exchange. Microporous Mesoporous Mater 2006; 91(1-3):78–84.

[111] Rallapalli P, Prasanth KP, Patil D, Somani RS, Jasra RV, Bajaj HC. Sorption studies of CO2, CH4, N2, CO, O2 and Ar on nanoporous aluminum terephthalate [MIL-53 (Al)]. J Porous Mater 2011;18(2):205–10.

[112] Hassanpouryouzband A, Joonaki E, Edlmann K, Heinemann N, Yang J. Thermodynamic and transport properties of hydrogen containing streams. Sci Data 2020;7. https://doi.org/10.1038/s41597-020-0568-6.

[113] Aftab A, Hassanpouryouzband A, Xie Q, Machuca LL, Sarmadivaleh M. Toward a Fundamental Understanding of Geological Hydrogen Storage. Ind Eng Chem Res 2022;61:3233–53. https://doi.org/10.1021/ACS.IECR.1C04380/ASSET/IMAGES/LARGE/IE1C04380_0009.JPEG.

[114] Hassanpouryouzband A, Adie K, Cowen T, Thaysen EM, Heinemann N, Butler IB, et al. Geological Hydrogen Storage: Geochemical Reactivity of Hydrogen with Sandstone Reservoirs. ACS Energy Lett 2022;7:2203–10. https://doi.org/10.1021/ACSENERGYLETT.2C01024/ASSET/IMAGES/LARGE/NZ2C01024_0004.JPEG.

[115] A. Raza M. Mahmoud S. Alafnan M. Arif G. Glatz H2, CO2, and CH4 Adsorption Potential of Kerogen as a Function of Pressure, Temperature, and Maturity IJMS 23 21 12767.

[116] Ali M, Yekeen N, Pal N, Keshavarz A, Iglauer S, Hoteit H. Influence of pressure, temperature and organic surface concentration on hydrogen wettability of caprock; implications for hydrogen geo-storage. Energy Rep 2021;7:5988–96.